REPORT DOCUMENTATION PAGE

AFRL-SR-AR-TR-08-0075

1. REPORT DATE *(DD-MM-YYYY)* 10-31-2007	2. REPORT TYPE Final	3. DATES COVERED *(From - To)* 15/08/2004 – 14/08/2007

4. TITLE AND SUBTITLE Multi-scale Computational Analyses of JP-8 Fuel Droplets and Vapors in Human Respiratory Airway Models	5a. CONTRACT NUMBER FA9550-04-1-0422
	5b. GRANT NUMBER
	5c. PROGRAM ELEMENT NUMBER
6. AUTHOR(S) Kleinstreuer, Clement <ck@eos.ncsu.edu>	5d. PROJECT NUMBER
	5e. TASK NUMBER
	5f. WORK UNIT NUMBER

7. PERFORMING ORGANIZATION NAME(S) AND ADDRESS(ES) North Carolina State University Raleigh, NC 27695-7910	8. PERFORMING ORGANIZATION REPORT NUMBER

9. SPONSORING / MONITORING AGENCY NAME(S) AND ADDRESS(ES) Dr. Walter J. Kozumbo/NL AFOSR Chemistry & Life Sciences 4015 Wilson Blvd., Rm712 Arlington, VA 22203-1954	10. SPONSOR/MONITOR'S ACRONYM(S)
	11. SPONSOR/MONITOR'S REPORT NUMBER(S)

12. DISTRIBUTION / AVAILABILITY STATEMENT Distribution A: Approved for Public Release

The U.S. Government is authorized to reproduce and distribute reprints for Governmental purposes notwithstanding any copyright notation thereon.

13. SUPPLEMENTARY NOTES

14. ABSTRACT

Using representative human nasal, oral and tracheobronchial airway models, transient 3-D as well as equivalent steady-state solutions have been obtained for the transport and deposition of spherical particles and droplets as well as vapors. It should be noted that equivalence to transient airflow and particle deposition results was achieved by employing matching Reynolds and Stokes numbers for steady-state simulations. Inhalation inlet conditions and aerosol characteristics resembled JP-8 fuel exposure scenarios in most case studies. Specifically, the following major tasks have been accomplished: (i) Airflow and transport/deposition of micron- and nano-size aerosols in representative human nasal airways; (ii) multi-component and/or impure droplet evaporation or hygroscopity; (iii) deposition differences between fuel aerosols (i.e., droplets) vs. vapors; (iv) studies of JP-8 fuel vapor transport and deposition by considering airway wall absorption; and (v) optimal drug-aerosol targeting.

The 3-year-project results are documented in 17 peer-reviewed journal articles (14 published and 3 accepted or submitted) and 9 conference papers/presentations. The often quoted articles have a significant impact on toxic/therapeutic aerosol research worldwide. Furthermore, in conjunction with other AFOSR-funded scientists, this work contributes to the understanding of health effects of inhaled JP-8 fuel aerosols and possible remedies, both

15. SUBJECT TERMS

JP-8 fuel droplets, vapor; human lung deposition; computational fluid-particle dynamics; aerosol deposition efficiencies; vapor surface concentration

16. SECURITY CLASSIFICATION OF:			17. LIMITATION OF ABSTRACT	18. NUMBER OF PAGES	19a. NAME OF RESPONSIBLE PERSON Clement Kleinstreuer
a. REPORT U	b. ABSTRACT U	c. THIS PAGE U	UU	32	19b. TELEPHONE NUMBER *(include area code)* 919-515-5261

Standard Form 298 (Rev. 8-98)
 Prescribed by ANSI Std. Z39.18

Table of Contents

Multi-scale Computational Analyses of JP-8 Fuel Droplets and Vapors in Human Respiratory Airway Models

1. Technical Summary

1.1 INTRODUCTION

Liquid and solid microparticles as well as nanoparticles and vapors are encountered in the ambient air and at the workplace, or are generated by inhalers as drug aerosols for therapeutic purposes. For example, because Jet-Propulsion fuel 8 (JP-8) is currently in use world-wide, especially in the US, Air Force personnel and people living near airfields may be exposed to JP-8 vapors as well as mixed vapor and aerosols during aircraft fueling, maintenance operations, cold starts, etc. (NRC, 2003; Ritchie et al., 2003). Such particles are inhaled through the extrathoracic and tracheobronchial airways, possibly down into the alveolar region. A certain percentage may deposit by touching the moist airway surfaces in various lung regions and hence are available for interactions with pulmonary tissue (Gehr & Heyder, 2000). As a result, toxic particles, such as JP-8 fuel aerosols, may induce pulmonary and other diseases (Frampton, 2001; Singh & Davis, 2002; NRC, 2003; ATSDA, 2005). Given any set of ambient conditions in terms of pollutant concentration, temperature and humidity, it is of interest to predict *how much deposits where* in the human respiratory tract under realistic breathing conditions. Such results, usually obtained via experimentally validated computer simulations, are of great interest to toxicologists, epidemiologists, health care providers, and regulators of air pollution standards.

In continuation to our previous AFOSR-contract work entitled "Computational Analysis and Simulation of Toxic Particle Deposition in the Human Respiratory System" (Award No. F49620-01-1-0492), the following work has been accomplished during the current funding period from 08/15/04 to 08/14/07:

(i) Inclusion of the human nasal cavity to compare particulate matter (PM) deposition between nasal and oral inhalation.

(ii) Analyses of geometric variations in lung morphology to investigate the impact of subject variability on PM and vapor deposition in terms of airway location and local concentration.

(iii) Development of models of droplet evaporation and hygroscopic growth, as well as a realistic JP-8 fuel surrogate in order to track at least 12 components, i.e., chemical markers, considered to be most harmful.

(iv)   Model development and analysis of absorption and intra-wall transport of nano-size particles and fuel vapor components.

(v) Development of the methodology for optimal drug aerosol targeting.

(vi) Development of particle deposition correlations for improved global lung deposition models.

The resolution and accuracy of the computed particle deposition pattern and aerosol concentrations on the airway surfaces are unsurpassed; in fact, such details cannot be obtained experimentally. As far as fuel aerosols are concerned, their toxicity level precludes human testing anyway. The completed work is an essential part of the AFOSR-sponsored toxicokinetics analyses employing physiologically based pharmacokinetic modeling procedures. Furthermore, it is applicable to "dosimetry-and-health-effect" studies being conducted by the U.S. EPA and "targeted drug aerosol delivery" of interest to the medical device and pharmaceutical industries.
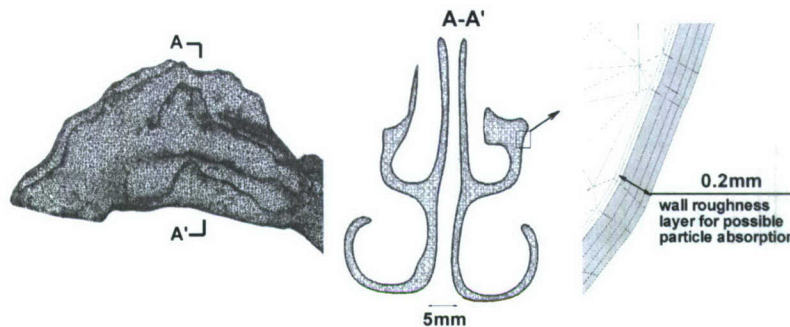
1.2 THEORY

1.2.1 Airway geometry

The representative airways models used for computer simulations include a nasal airway model, an oral-tracheobronchial airway model, an alveolar duct, and repeated triple bifurcation units (Fig. 1). The representative nasal airway geometry was obtained from widely used MRI files of the nose of a healthy, 53-year-old, nonsmoking male (73 kg mass, 173 height), provided by CIIT (Research Triangle Park, NC). The detailed description of the nasal airway model is given by Shi et al. (2006), while the oral-tracheobronhcial airway model is described in Li et al. (2007), and Kleinstreuer & Zhang (2003). The alveolated duct model is based on the geometric data provided by Haefeli and Weibel (1988), characterized by smooth cells or sacs, which are also related to the actual shapes of alveoli (see Li and Kleinstreuer, 2007).

The dimensions of the four-generation (i.e., triple bifurcation) airway units are similar to those given by Weibel (1963) for adults with a lung volume of 3500ml. The tracheobronchial airways (TB region), in terms of G0-G15, can be subdivided into five blocks or levels which are approximated by "triple-bifurcation units" (TBUs) (see Fig. 1d). The idea is to extend the TBUs extend "in series" as well as "parallel" after appropriate modifications, in order to capture actual lung morphologies of healthy adults. Specifically, air-particle outflow conditions of an oral airway model (see Zhang et al., 2005) can be adjusted as inlet conditions for G0-G3, which at their outlets are again adjusted to become inlet conditions for G3-G6, etc. Necessary adjustments would include: (a) the magnitudes of velocity and turbulence quantities which are recalculated due to the variation in branch tube diameters to capture "subject variability"; and (b) the profiles
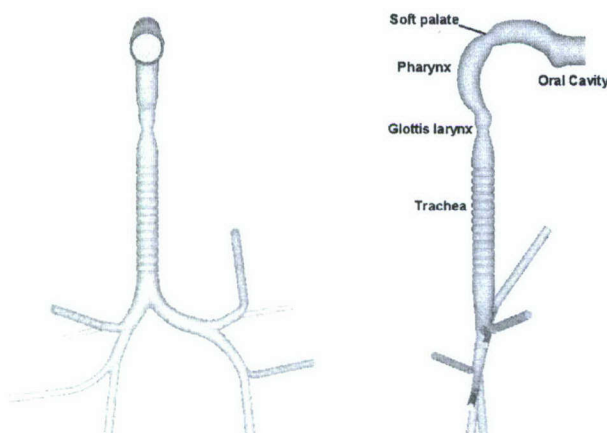
of variables are also reconstructed and rotated to some degree for the inlet to the downstream airway unit to incorporate the non-planar geometry effect.
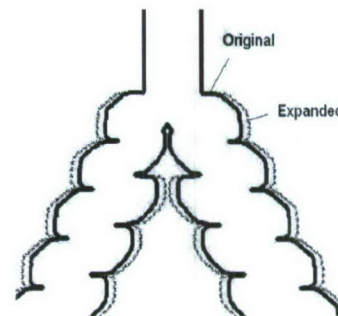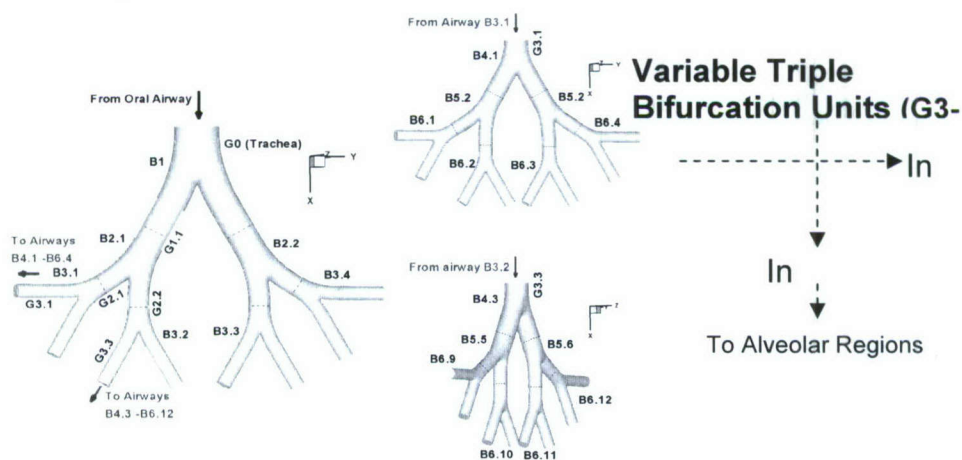
(a) Nasal airway model

(b)Oral-tracheobronchial airway model

(c) Alveolated duct

(d) Repeated triple bifurcation units

Fig.1: Models of human respiratory systems

3

1.2.2 Governing equations

Airflow. In order to capture the airflow structures in the laminar-to-turbulent flow regimes, i.e., $0 < Re_{local} < 10,000$ for the maximum (transient) inhalation flow waveform, the low-Reynolds-number (LRN) k-ω model of Wilcox (1998) has been selected and adapted which has been demonstrated to be appropriate for such internal flows. All air transport equations, including the heat transfer equation, as well as initial and boundary conditions are given in Zhang & Kleinstreuer (2003a, b) and Kleinstreuer & Zhang (2003). The effect of wall roughness (see Fig.1a) on the laminar flow profile in the nasal cavity is included in the airflow simulations by introducing the roughness-viscosity (υ_R) in a manner similar to the eddy-viscosity (Shi et al., 2007a). Based on experimental correlations and analytical considerations, a set of equations to calculate υ_R in microtubes with certain wall roughness (Mala & Li, 1999) have been proposed.

Transport of micro-size droplets. With any given ambient concentration of non-interacting spherical droplets, a Lagrangian frame of reference for the trajectory computations of the evaporating droplets can be employed. The detailed descriptions of micro-particle trajectory equation with turbulent dispersion are given in Zhang et al. (2005).

Droplet evaporation or hygroscopic growth. This analysis considers that the droplet temperature and composition are maintained spatially uniform but evolve with time and the droplet remains spherical during vaporization. This assumption is reasonable because of the small Biot number (Bi<<1) for the micro-size droplets. Considering the convective heat and mass transfer over the whole surface of the spherical droplets, the change in droplet mass (or size) can then be calculated (Longest and Kleinstreuer, 2005; Zhang et al., 2006b).

Mass transfer of vapor or nanoparticles. The convection mass transfer equation of ultrafine particles, or (JP-8) fuel vapor, whose dominant radial transfer mechanisms are Brownian motion and turbulent dispersion is given in Zhang & Kleinstreuer (2003b, 2004).

Assuming that the airway wall is a perfect sink for aerosols or vapors upon touch, the boundary condition on the wall is $Y_w=0$. This assumption is reasonable for fast gas-wall reaction kinetics (Fan et al., 1996), or vapors of high solubility and reactivity, and also suitable for estimating the maximum deposition of toxic vapor in the airways. For less soluble vapors, the wall concentration would be greater than zero so that transport in tissue and in airways must be considered simultaneously for simulating vapor uptake. Assuming that the surface of respiratory epithelium is covered by a mucus layer with uniform thickness and a lipid layer lie below the mucus lining simulating the transport barrier by the epithelial cell membrane, Keyhani et al. (1997) derived a flux condition at the airway boundary including the vapor transport in the

4

tissue. This boundary condition was inferred from the mass conservation and mass diffusion of vapor from the airway to the mucus layer and to the tissue, which is given as:

$$D_{in} \frac{\partial Y}{\partial n} + KY = 0 \tag{1}$$

where D_{in} is the inlet tube diameter, n is the direction normal to the airway wall, and K is a dimensionless parameter, here we call it absorption parameter, which is defined as

$$K = \frac{D_{in} \tilde{D}_m \xi}{\tilde{D}_a \beta \tanh(\xi H_m)} \left[1 - \frac{2\tilde{D}_m / H_m}{(\tilde{D}_m / H_m + P_l)(e^{\xi H_m} - e^{-\xi H_m})} \right] \tag{2}$$

where $\tilde{D}_a, \tilde{D}_m$ are the vapor diffusivity in the air and the liquid mucus phase, respectively; H_m is the thickness of the mucus layer; and β is the equilibrium partition coefficient for a given contaminant molecular, which can be determined by Henry"s law; $\xi = \sqrt{k_r / \tilde{D}_m}$ with k_r being a single rate constant considering the chemical reactions of vapors in the mucus layer; $P_l = \gamma \tilde{D}_l / H_l$ is the lipid permeability coefficient with $\gamma, \tilde{D}_l, H_l$ being lipid-mucus partition coefficient, vapor diffusivity in the lipid and the thickness of the lipid layer, respectively.

Clearly, for a highly soluble ($\beta \to 0$) or high reactive ($k_r \to \infty$) vapor, the boundary condition (1) reduces to Y=0. If vapor is insoluble ($\beta \to \infty$), the boundary condition reduces to the zero mass flux condition, i.e., $\partial Y / \partial n = 0$. Ignoring removal of contaminant molecules in the mucus by chemical reaction and the resistance to transport across the lipid barrier, the absorption parameter K reduces to:

$$K = \frac{D_{in} \tilde{D}_m}{\tilde{D}_a \beta H_m} \tag{3}$$

Deposition parameters. The regional deposition of micron particles in human airways can be quantified in terms of the deposition fraction (DF) or deposition efficiency (DE) in a specific region (e.g. oral airway, first, second and third bifurcations etc.); they are defined as:

$$DF_{particle} = \frac{Number\ of\ deposited\ particles\ in\ a\ specific\ region}{Number\ of\ particles\ entering\ the\ mouth} \tag{4}$$

$$DE_{particle} = \frac{Number\ of\ deposited\ particles\ in\ a\ specifc\ region}{Number\ of\ particles\ entering\ this\ region} \tag{5}$$

In addition to the above two traditional deposition parameters DE and DF, a deposition enhancement factor (DEF) is considered to be employed to quantify local particle deposition patterns (Zhang et al., 2005). The DEF is defined as the ratio of local to average deposition

densities, i.e.,

$$DEF = \frac{DF_i / A_i}{\sum_{i=1}^{n} DF_i / \sum_{i=1}^{n} A_i} \tag{6}$$

where A_i is the area of a local wall cell (i), n is the number of wall cells in one specific airway region and DF_i is the local deposition fraction in the local wall cell (i). *Clearly, the presence of high DEF-values indicates inhomogeneous deposition patterns, including "hot spots" in terms of locally maximum particle depositions.*

The deposition fraction (DF) of nanoparticles can also be calculated with the regional mass balance or the sum of local wall mass flux with the Eulerian-Eulerian modeling technique. As for the local wall mass flux of nanoparticles, it can be determined as

$$\dot{m}_w = \rho A_i j_{wall,i} \tag{7}$$

where A_i is the area of local wall cell (i) and $j_{wall,i}$ is the particle flux at the local wall cell given by

$$j_{wall,i} = -D_p \frac{\partial Y}{\partial n}\bigg|_{wall,i} \tag{8}$$

The local particle deposition fraction (DF) or deposition efficiency (DE), which is defined as the ratio of local wall mass flux to the inlet mass flux, can be expressed as

$$DF_{local} \text{ or } DE_{local} = (A_i j_{wall,i})/(Q_{in} Y_{in}) \tag{9}$$

and the regional DF or DE can be determined as

$$DF_{region} \quad \text{or} \quad DE_{region} = \sum_{i=1}^{n} (A_i j_{wall,i})/(Q_{in} Y_{in}) \tag{10}$$

where n is the number of wall cells in one specific airway region, e.g., oral airway, first airway bifurcation, etc. The subscript "in" refers to mouth inlet for calculating DF, while it refers to the inlet at one specific airway bifurcation for calculating DE. The local nanoparticle deposition patterns can also be quantified in terms of the deposition enhancement factor (DEF), i.e.,

$$DEF = j_{wall,i} / [\sum_{i=1}^{n} (A_i j_{wall,i})/\sum_{i=1}^{n} A_i] \tag{11}$$

Again, the DEF will indicate particle deposition "hot spots" in certain regions.

1.2.3 Numerical method

Different numerical approaches were used for modeling the airflow and particle transport in different representative airway models. The numerical simulations in the nasal airway model were carried out with a user-enhanced commercial finite-volume based program, i.e., CFX 5.7 from Ansys Inc (Canonsburg, PA). The details can be found in Shi et al. (2007b). It should be noted that, based on experimental data, the "wall-roughness-region-enhanced-particle-capturing-effect" was incorporated into the computation with a 0.2mm wall roughness layer which is 100% penetratable for particles less than 4μm and captures all particles larger than 4μm in diameter. The numerical solutions of airflow and particle transport in the oral and tracheobronchial airways

were carried out with a in-house CFPD code or user-enhanced finite-volume based program CFX4.4 from Ansys, Inc., and an off-line parallelized particle transport code "F90" (for details see Zhang et al., 2005; Li et al., 2007). While CFPD code and CFX Version 4 is a solver based on structured meshes, CFX5 & 10 use unstructured meshes to accommodate more complex geometries.

The airflow and particle transport in the 2-D alveolar duct model was simulated with the lattice Boltzmann method (LBM) (see Li and Kleinstreuer, 2007). LBM is a mesoscopic method that covers the range between molecular dynamics and the familiar continuum mechanics solvers. LBM is a computational approach relies upon fluid-element (i.e., "particle") movement and collision. Instead of tracking individual "particles", LBM evaluates a distribution function (i.e., the probability of finding a particle at a given location at a given time) in light of particle motion and collision. This approach eliminates the statistical noise. The detailed simulation processes are described in Li and Kleinstreuer (2007).

The mesh topologies of the three airway models were determined by refining the meshes until grid independence of the flow field and particle deposition fraction solutions were achieved. All computations were performed on high performance computers at Army Research Lab (ARL), an IBM Linux Cluster with 175 dual Xeon compute nodes at North Carolina State University's High-Performance Computing Center (Raleigh, NC) and local dual Xeon Intel 3.0G Dell workstations (CFPD Laboratory, Department of Mechanical and Aerospace Engineering, NC State University).

1.3 RESULTS

Some selected computational results including model validations are presented in this section. More results and detailed descriptions can be found in relevant publications (see Sect.2).

1.3.1 Model validations

For accurate computational fluid-particle dynamics (CFPD) simulations, matching comparisons with theoretical or experimental fluid velocity profiles, pressure drops and local particle distributions are necessary. As listed in Table 1, our CFPD modeling has been extensively validated with various experimental data sets. For example, CFPD (then CFX4) for steady and transient laminar flows in bifurcations by Comer et al. (2000, 2001); Zhang & Kleinstreuer (2002); and Zhang et al., (2001b) and for laminar, transitional and turbulent flows in tubes with local obstructions by Kleinstreuer & Zhang (2003), and Zhang & Kleinstreuer (2003a). Especially, the low-Reynolds-number (LRN) k-omega model has been extensively validated and has been proven to be an applicable approach to capture the velocity profiles and turbulence
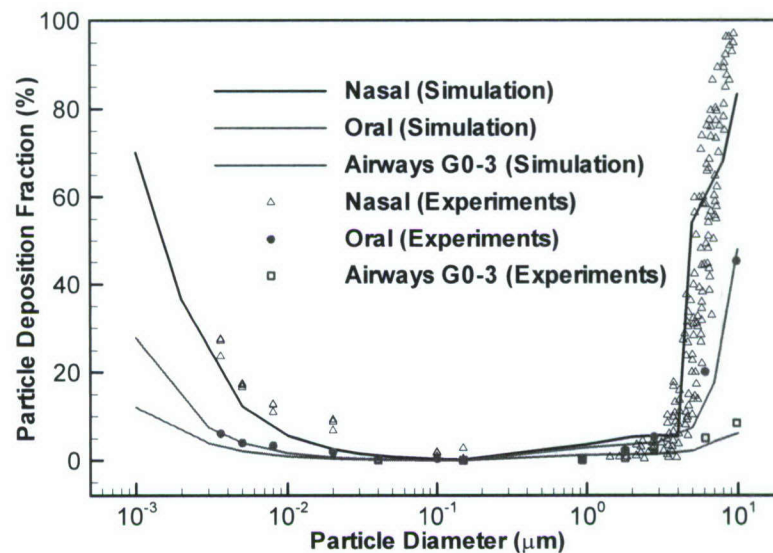
kinetic energy for laminar-transitional-turbulent flows in the constricted tubes of the upper airways (see Zhang & Kleinstreuer, 2003a). Similarly, past simulated spherical, micro-particle depositions in airways were successfully compared with measured deposition efficiencies and deposition patterns (Comer et al., 2000; Zhang et al., 2002a-d) . The simulation of spherical, nanoparticle deposition due to diffusional transport has been validated with both analytical solutions in straight pipes and experimental data for a double-bifurcation airway model (Shi et al., 2004) as well as experimental data in an oral airway model (Zhang & Kleinstreuer, 2003b). In addition, the comparisons conducted by other researchers in terms of their experimental measurements or approximate analytical solutions also show that the previous simulated velocity profiles and deposition data in human airways published by the PI and his co-workers are accurate and reliable (see Fresconi et al., 2003; Broday, 2004). Two examples are given in Figs. 2 and 3 for micron particle deposition in the human upper airways and micron particle transport in a human oral airway model.

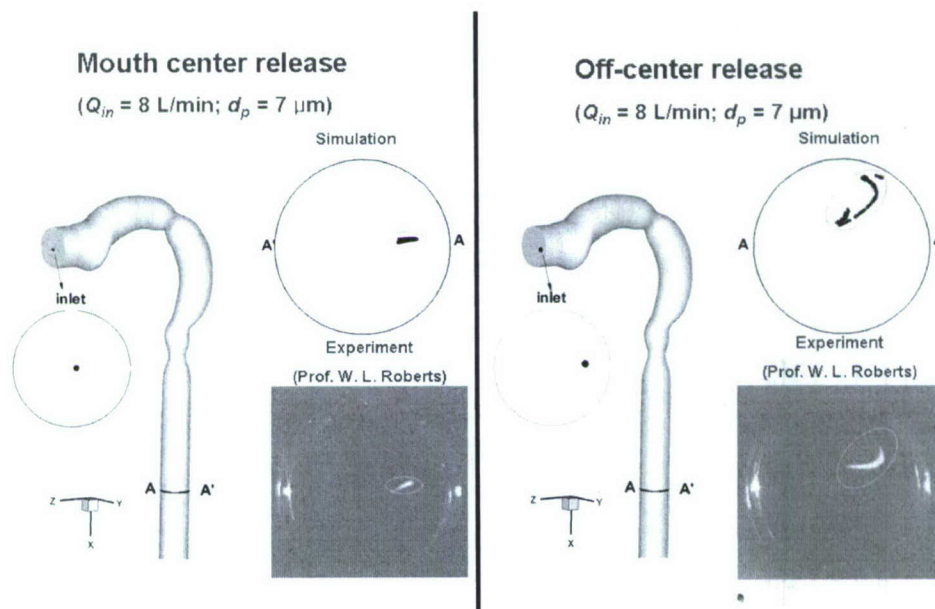**Table 1 List of Validated CFPD models**

Submodel	Description	Geometry	References
Air flow	Laminar-transitional-turbulent airflows	Constricted tube	Kleinstreuer & Zhang (2003); Zhang & Kleinstreuer (2003a)
	Steady and transient laminar flows	Single bifurcation tube	Comer et al. (2001); Zhang & Kleinstreuer (2002)
Micro-size particle/droplet transport and deposition	Steady inspiratory particle distributions, deposition patterns and efficiencies	Double bifurcation airway model, oral airway model, nasal cavity, curved bend	Comer et al. (2000); Shi et al. (2004); Zhang et al. (2001a,b, 2002a-d,2005)
	Cyclic particle deposition	Double bifurcation airway model	Zhang et al. (2002a-d)
Droplet evaporation	Convection vaporization of water and single-component JP-8 fuel droplets	Human lung airways (cast model) mouth to G3	Zhang et al. (2004, 2006b)
Spherical nanoparticle deposition	Steady and transient deposition efficiencies with different airflow rates	Straight tube, curved tube, double bifurcation airway model, tracheobronchial airway model, oral airway model, nasal cavity	Shi et al. (2004, 2006); Zhang & Kleinstreuer (2003); Zhang et al. (2005)
Interaction of airflow and microparticle trajectories in alveolated duct	Transient laminar 2-D fluid-particle dynamics in expanding/contracting cells	Bifurcating, alveolated duct	Li & Kleinstreuer (2007)

In summary, the good agreements between experimental findings and theoretical predictions instill confidence that the present computer simulation model is sufficiently accurate to analyze transport and deposition of toxic particle/droplet and vapor in three-dimensional representative airway models associated with laminar-to-turbulent airflows.
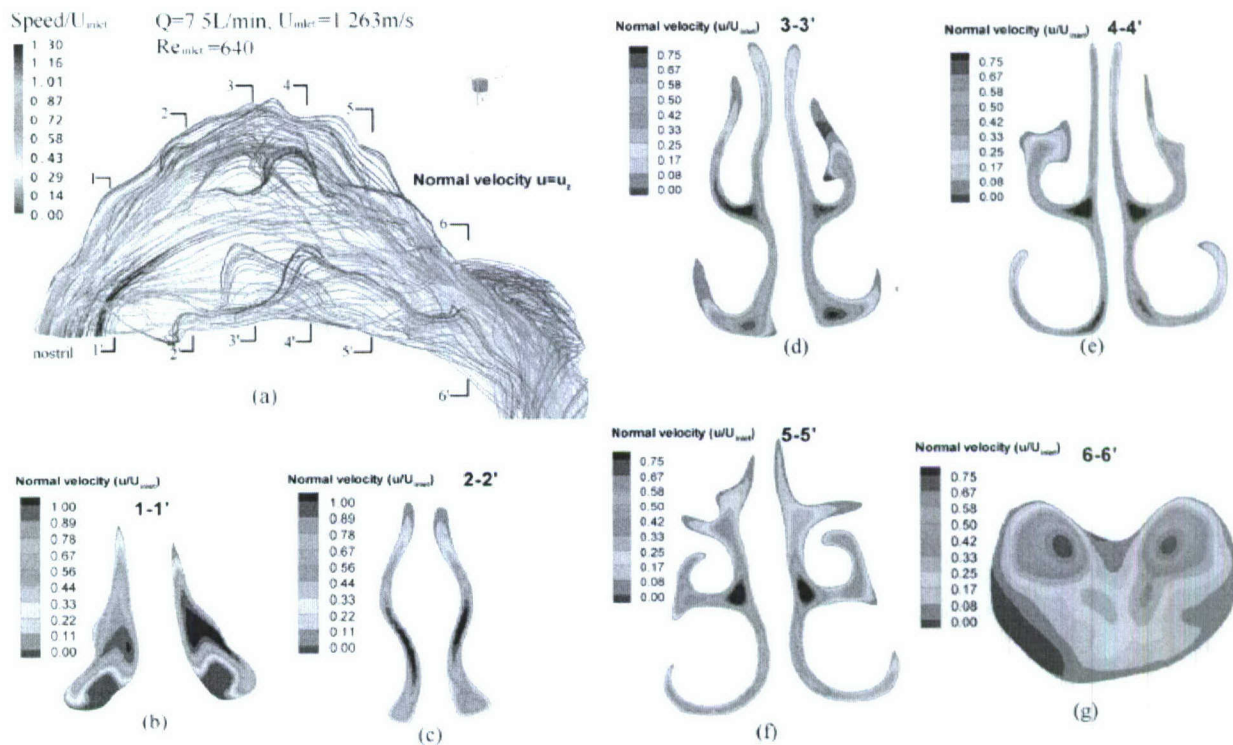

Fig. 2: Experimentally validated computer simulation results of particle deposition fractions in human upper airways as a function of particle size.

Fig. 3: Comparisons of simulated and measured particle distributions with different inlet release positions

1.3.2 Airflow and particle deposition in the human nasal cavities

Airflow patterns. A typical inspiratory airflow structure in the human nasal cavities is given in Fig. 4 assuming steady laminar flow under resting condition (Q=7.5 L/min). After the airflow enters a nasal cavity, the majority of flow passes through the middle-to-low portion of the main passageway between middle and inferior meatuses (see. Figs. 8 d-f). Especially, two high speed regions are located under the middle and inferior meatuses. The narrow olfactory region and the upper part of the middle and inferior regions receive only small amounts of air, which is believed to protect the cells for the sense of smell. Although airflow enters the nose almost vertically, the quasi-funnel shape of the vestibule redirects the airflow horizontally after the nasal valve, i.e., towards the lower nasal passageway. Then, most of the inhaled air flows through the wider middle-to-low portion of the main passageway which is free of obstacles. The secondary flow fields are quite strong in the middle part of the nasal cavities, i.e., Slices 3-3' and 5-5' because of the locally complex geometric features and the airflow direction changes in the vestibule (see Shi et al., 2008).

Figure 4. Velocity fields in human nasal cavity at constant inlet flow rate of 7.5L/min: (a) 3-D streamlines and velocity contours (b-g) Velocity fields in six selected slices

Vapor or nanoparticle deposition. Most particles, or equivalent vapors, of $d_p = 1nm$ pass through the middle-to-low main passageway convected by the main airflow portion. Especially a high particle concentration is observed in the main passageway below the middle meatus. However, as the flow rate increases, a larger portion passes through the olfactory region (Shi et al., 2008). Figure 5 depicts the distributions of the deposition enhancement factor (DEF) for quasi-steady flow rate of 7.5L/min and particle sizes $d_p = 1nm$, and 5nm. Specifically, for $d_p = 1nm$ (or vapor), the majority of deposition occurs in the anterior part of the nasal cavity because of the high diffusivity. The meatuses regions experience only small deposition fluxes because most particles are taken up before they can reach the deeper regions of the meatuses. In Figs. 15 and 16, high DEF values can be seen around the nasal valve region due to the locally narrowing airway. The top views of Fig. 5b, where the middle meatus emerges, reveal the highest DEF values. Overall, 90% of the incoming 1nm-particle (or vapor) mass deposits if a perfect absorbing airway wall is assumed. The effects of mucus layer and airway wall absorption is discussed by Shi et al. (2008). For $d_p = 5nm$ (see Fig.5c, d), deposition fluxes are a bit more evenly distributed because of the somewhat uniform particle concentrations in the airways. Still, the locations of deposition "hot spots" are basically the same, i.e., the nasal valve region and middle-meatus zones feature the highest DEF values.

When investigating the nanoparticle deposition efficiency and the fraction of deposited mass in the meatus regions, it was found that the middle meatus experiences a higher deposition efficiency and the fraction of deposited mass than the inferior meatus because many more nanoparticles pass through the middle meatus region. For example, when $d_p = 1nm$ and Q=7.5L/min, the middle meatus features a deposition efficiency of about 18% while in the inferior meatus it is only 9%, although the surface area of the middle meatus is only about 33% larger than that of the inferior meatus. However, it is surprising to find that for both meatuses, despite of some occasional differences, their fractions of deposited mass are almost constant throughout the particle size range of 1 nm$\leq d_p \leq$150 nm and three flow rates, i.e., Q=7.5, 10 and 20L/min. Especially for the middle meatus, the fraction of deposited mass is consistently around 19-20%. The olfactory region is the most desirable target for drug delivery in the human nasal cavity; but, it is also the most vulnerable to toxic aerosols (see Illum, 2003). Very small amounts of nanoparticles deposit onto the olfactory surfaces. For example, when Q=7.5L/min, the deposition efficiency is only 0.2% in the olfactory region for 1nm particles (or vapor).

In terms of simulated results, the laminar nanoparticle deposition efficiency in the human nasal cavity can be expressed as

$$\eta_d^{Lam} = C \cdot (\frac{D_p L \cdot \pi}{4 \cdot Q})^{1/2} \cdot Sc^{-1/6}$$

(12)

where Sc is the Schmidt number, L$\approx$10cm is the equivalent nasal airway length and C is a curve-fitted coefficient representing geometric complexities, given as

$$C = a + b \cdot \ln \Delta$$

(13)

where Δ is the diffusion parameter ($\Delta = \frac{D_p L}{4UR^2}$), $a = 0.568$ and $b = -0.69$ for 7.5$\leq$Q$\leq$20L/min and 1 nm$\leq d_p \leq$150 nm.

Figure 5: Deposition Enhancement Factor (DEF) contours at constant inlet flow rate of 7.5L/min for (a,b) 1nm-particles (vapor), and (c,d) 5nm-particles.

Micron particle deposition. Usually, replicas of nasal airways with coarser manufacturing methods (rough walls) or in vivo nasal airways produce higher deposition efficiencies than physical models produced with fine manufacturing procedures (smooth walls) (Kelly et al., 2004). As shown in Fig. 6a, ignoring the wall roughness layer underestimates total deposition efficiencies significantly while simulations incorporating the wall roughness layer effect generate a good agreement with the measurements Kelly et al. (2004). In summary, Fig. 6 strongly indicates the important influence of the wall roughness region on particle deposition in the nasal cavity.

Clearly, the particle deposition efficiency increases with higher IP-values ($IP=Qd_p^2$), predominantly in the nasal valve region. Specifically, Fig. 7 shows the particle deposition patterns for different inlet conditions. When $d_p = 2\mu m$, only a small amount of particles deposit in a scattered fashion (see Fig. 7a, b). When $d_p = 10\mu m$, more particles deposit due to an increase in impaction (see Fig. 7c, d). Basically, there are three major deposition hot spots. The first one is near the nasal valve where a narrow and 90-degree funnel-shaped bend form the stagnant point for many particles. The second one is the top of the middle meatus wall. With a steep geometry change, the particles intend to hit the middle meatus wall or middle turbinate

12

because of direct impaction and secondary flows. The third site is near the nasopharynx where the nasal airways experience a third 90-degree bend after a constriction so that particles hit the wall due to the combined effects of centrifugal force, jet flow and inertial impaction.
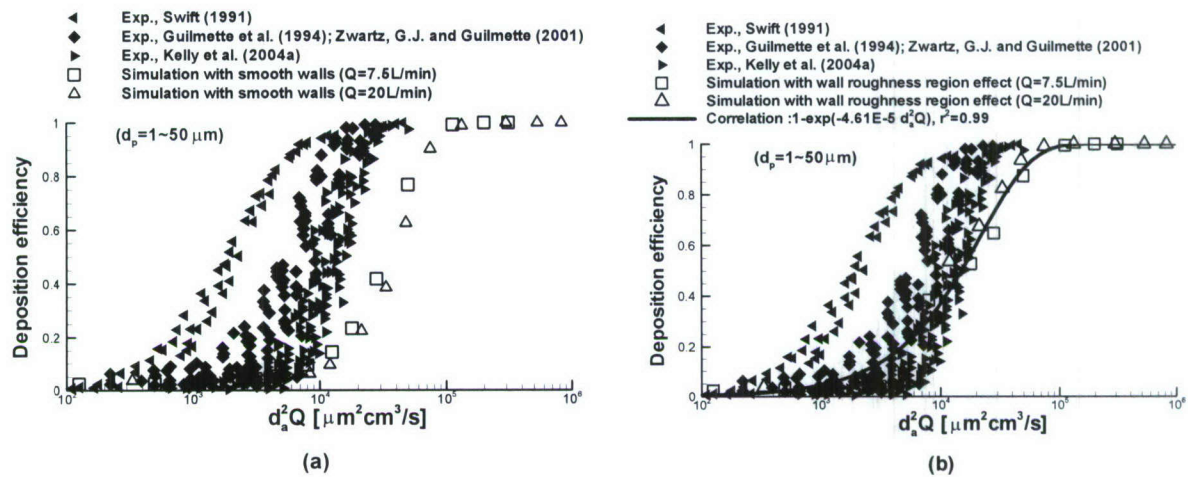

Figure 6: Particle deposition efficiency comparison between present simulation and experiments (Shi et al., 2007)
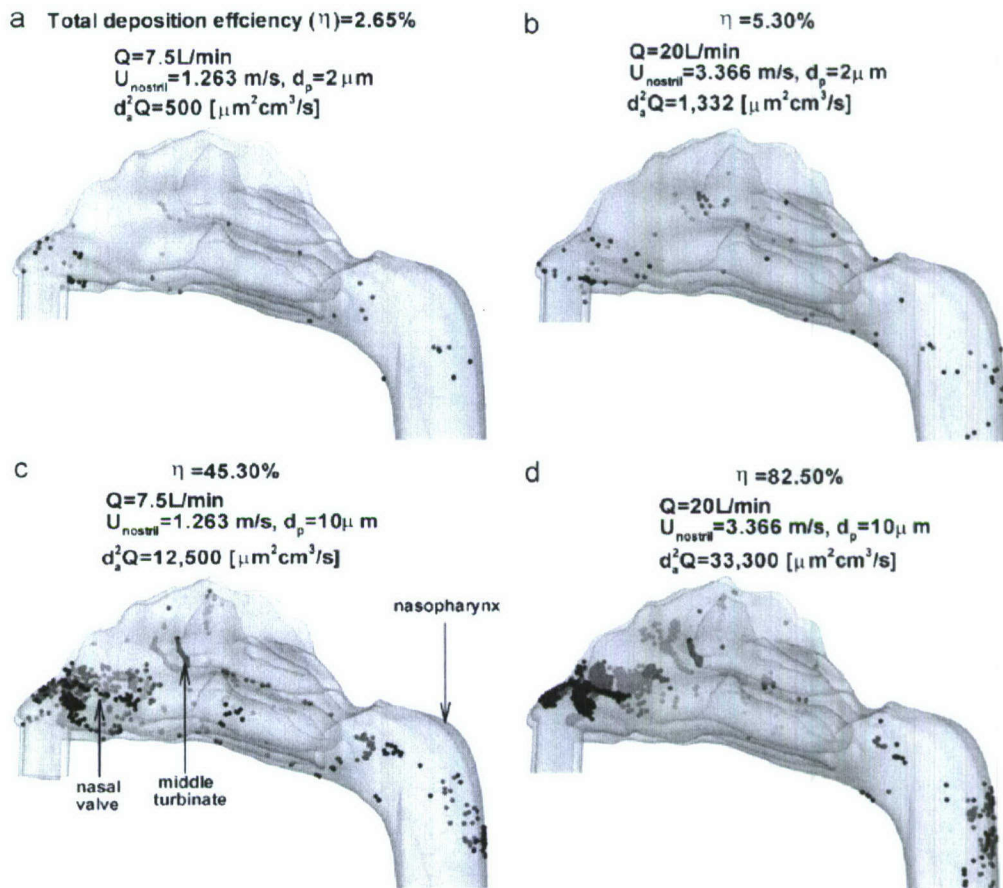

Figure 7: Particle deposition patterns for different inlet conditions

13

Based on the simulation results, a correlation function was developed to predict the total particle deposition efficiency in human nasal cavities. Figure 6b also includes a correlation for the deposition efficiency as a function of impaction parameter, IP. The correlation can be written as an exponential function (Shi et al., 2007):

$$\eta = 1 - \exp(a \cdot IP) \tag{14}$$

where $a = 4.61 \times 10^{-5}$ and $IP = d_a^2 \cdot Q$. The resulting r^2 is 0.99 indicating a good fit.

1.3.3 Deposition comparisons between vapor (nanoparticles) and micron particles (droplets)

Typical deposition patterns of both nano- and micron- particles are shown in Fig. 8 in terms of DEF-distributions in oral and bifurcation airway models. Micron particle deposition during inhalation is mainly due to impaction, secondary flow convection, and turbulent dispersion. Thus, they largely deposit at stagnation points for axial particle motion, such as the tongue portion in the oral cavity, the outer bend of the pharynx/larynx, and the regions just upstream of the glottis and the straight tracheal tube, as well as the regions of carinal ridges in the bronchial tree. As for nanoparticles, the enhanced deposition mainly occurs at the carinal ridges and the inside walls around the carinal ridges again due to the complicated air flows and large particle concentration gradients in these regions. Although the enhanced deposition sites (i.e., those with high DEF-values) in the bifurcating airways are similar for nano- and micro-size particles, the maximum DEF-values for nanoparticles are two to three orders of magnitude smaller than for microparticles. Specifically, the DEF_{max} for microparticles is of the order of 10^2 to 10^3, while DEF_{max} for nanoparticles is of the order of 1 (Zhang et al., 2005). A more uniform distribution of deposited nanoparticles may relate to a different toxicity effect when compared to fine particles made of the same materials. Specifically, not only the larger surface areas relative to the particle mass but also, more importantly, the larger surface areas with a *near-uniform* deposition can generate a higher probability of interaction with cell membranes. Hence, it may result in a greater capacity to absorb and transport toxic substances into tissue, blood and the whole body, and the enhanced possibility of systematic diseases, such as cardiovascular diseases (Hoet et al., 2004; Oberdorster et al., 2005). In contrast, the extremely high local DEF values for micron particles indicates the possibility of local pathological changes in bronchial airways, such as the formation of lung tumors (Balashazy et al., 2003).
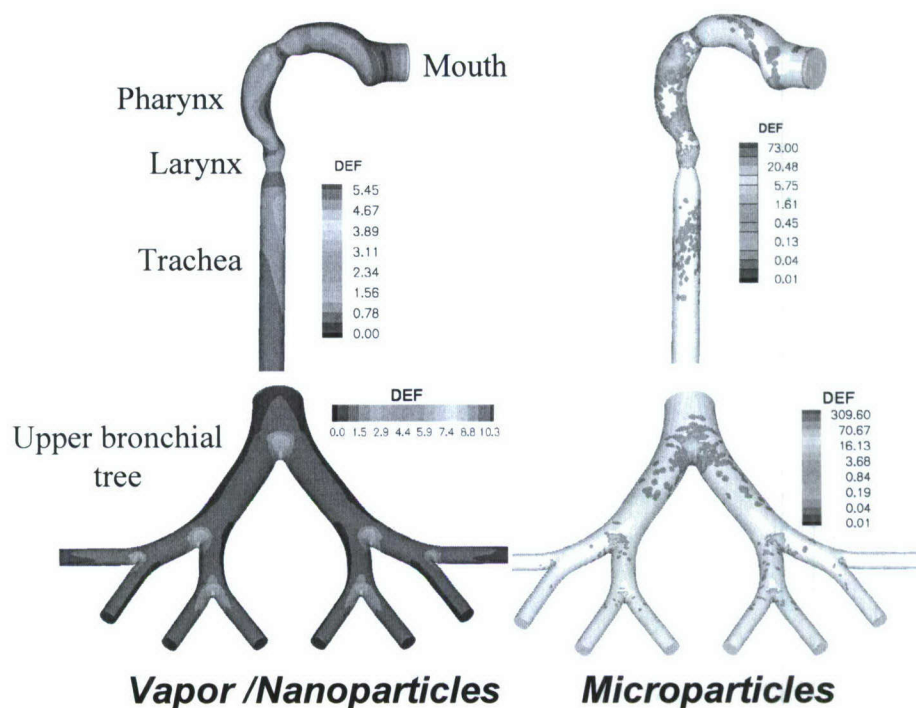
Mouth

Pharynx

Larynx

DEF
5.45
4.67
3.89
3.11
2.34
1.56
0.78
0.00

Trachea

DEF
73.00
20.48
5.75
1.61
0.45
0.13
0.04
0.01

DEF
0.0 1.5 2.9 4.4 5.9 7.4 8.8 10.3

Upper bronchial
tree

DEF
309.60
70.67
16.13
3.68
0.84
0.19
0.04
0.01

Vapor /Nanoparticles   **Microparticles**

Fig. 8: Local deposition patterns of nano- and micro-particles

1.3.4 Evaporation and deposition of multi-component droplets

Development of droplet vaporization model and JP-8 fuel surrogate. An effective model for predicting multicomponent aerosol evaporation in the upper respiratory system that is capable of estimating the vaporization of individual components is needed for accurate dosimetry and toxicology analyses. In this study, the performance of evaporation models for multicomponent droplets over a range of volatilities is evaluated based on comparisons to available experimental results for conditions similar to aerosols in the upper respiratory tract. Models considered include a semiempirical correlation approach as well as resolved-volume computational simulations of single and multicomponent aerosol evaporations to test the effects of variable gas-phase properties, surface blowing velocity, and internal droplet temperature gradients. Of the parameters assessed, concentration-dependent gas-phase specific heat had the largest effect on evaporation and should be taken into consideration for respiratory aerosols that contain high volatility species, such as n-heptane, at significant concentrations. For heavier droplet components or conditions below body temperatures, semiempirical estimates were shown to be appropriate for respiratory aerosol conditions. In order to reduce the number of equations and properties required for complex mixtures, a resolved-volume evaporation model was used to identify a twelve-component surrogate representation of potentially toxic JP-8 fuel based on comparisons to experimentally reported droplet evaporation data. Due to the relatively slow

evaporation rate of JP-8 aerosols, results indicate that a semiempirical evaporation model in conjunction with the identified surrogatemixture provide a computationally efficient method for computing droplet evaporation that can track individual toxic markers. However, semiempirical methodologies are in need of further development to effectively compute the evaporation of other higher volatility aerosols for which variable gas-phase specific heat does play a significant role.
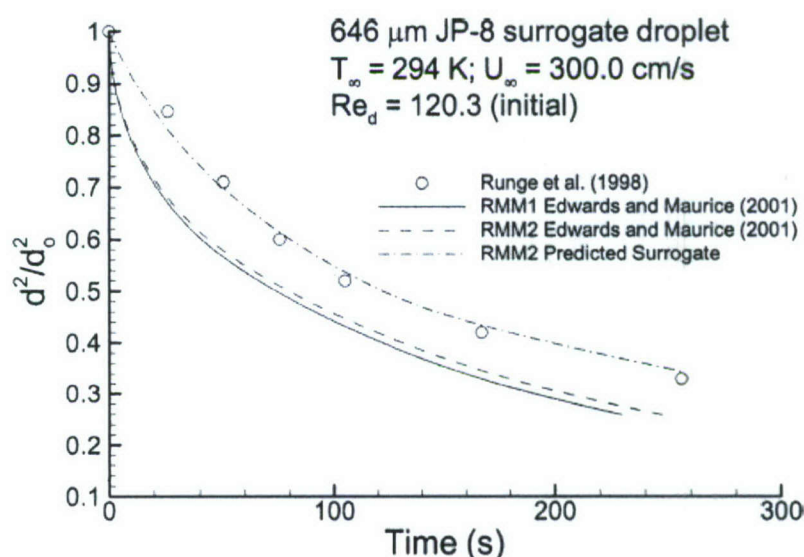
Table 2 Twelve component JP-8 surrogate

Component	Wt % Edwards and Maurice (2001)	Wt % Computed with RMM2
iso-octane	5.0	0.25
Methyl cyclohexane	5.0	0.25
m-xylene	5.0	0.25
Cyclooctane	5.0	0.25
Decane	15.0	7.0
Butyl benzene	5.0	3.0
1,2,4,5 tetramethyl benzene	5.0	14.0
Tetralin	5.0	15.0
Dodecane	20.0	23.0
1-methyl naphthalene	5.0	8.0
Tetradecane	15.0	17.0
Hexadecane	10.0	12.0

Solutions of selected evaporation models (i.e., RMM1 and RMM2) have been evaluated for a 12-component surrogate mixture suggested by Edwards and Maurice (2001) (Table 2) and are compared to the experimental results of Runge et al. (1998) (see Fig. 9 from Longest & Kleinstreuer, 2005). The significant discrepancy between the computed and empirical results is likely due to an incorrect surrogate mixture for droplet evaporation or inaccuracy of the assumed rapid mixing model for droplets consisting of a significant number of compounds. Inclusion of concentration gradients in the droplet will slow the initial evaporation rate by limiting transport of high volatility compounds to the surface, in the absence of Hill vortex formation. However, evaporation at later times will be increased due to continued availability of the lighter components. It appears that the slopes of the predicted evaporation curves remain greater than or equal to the experimental data. This indicates that internal gradients may not be responsible for the discrepancy between predicted and experimental values, which is consistent with the computed results for a binary heptane–decane droplet. Based on calculations with the RMM2
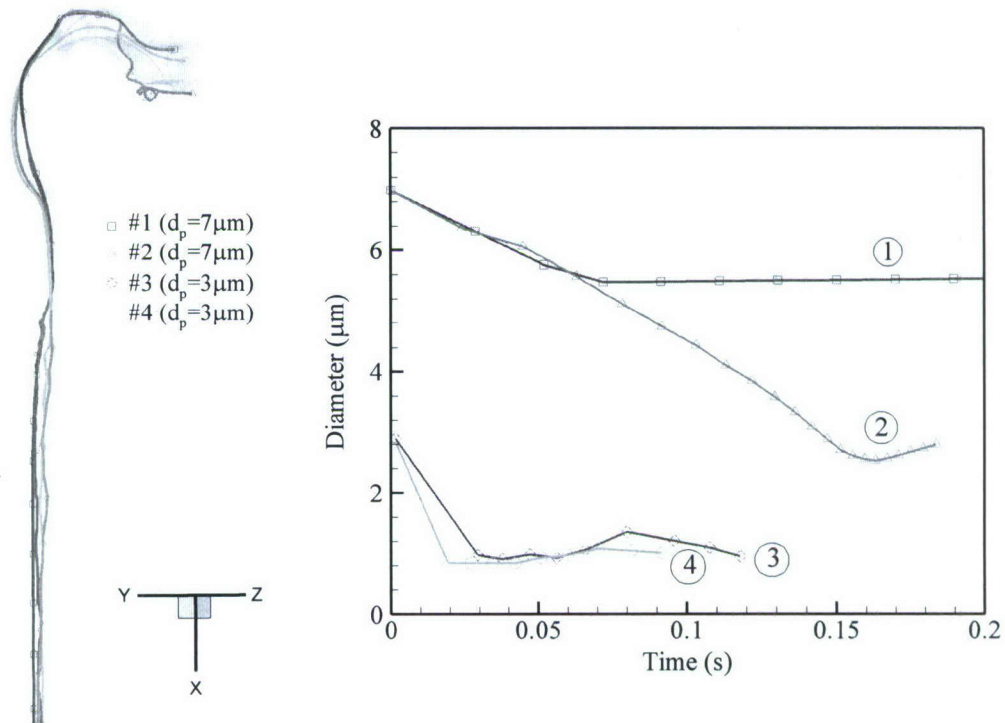
approximation, a surrogate mixture that accurately predicts droplet evaporation is defined in Table 2, and evaporation rates are shown in Figure 9. For the suggested surrogate model, differences among the RMM1 and RMM2 solutions are largely negligible, which indicates that either a reduced presence of volatile hydrocarbons or a reduced evaporation rate associated with multiple components minimizes the need to account for variable gas-phase specific heat in this case. As such, the ODE-based semiempirical solution used with the suggested surrogate mixture provides a computationally effective method for evaluating the evaporation of potentially toxic JP-8 aerosols in the respiratory tract.

646 μm JP-8 surrogate droplet
T_∞ = 294 K; U_∞ = 300.0 cm/s
Re_d = 120.3 (initial)

○   Runge et al. (1998)
——— RMM1 Edwards and Maurice (2001)
– – – RMM2 Edwards and Maurice (2001)
– · – · RMM2 Predicted Surrogate

Figure 9: Computational estimates of normalized droplet surface area (d^2/d_o^2) over time compared to the experimental results of Runge et al. (1998) for a twelve-component JP-8 surrogate mixture (Longest & Kleinstreuer, 2005).

Transport and deposition of multi-component droplets. The impurities of multi-component droplets may reduce the surface vapor pressure and hence decrease the droplet evaporation or cause droplet growth. As an example, the evaporation/ hygroscopicity , transport and deposition of isotonic and hypertonic saline droplets have been simulated for the human upper airways and analyzed for different steady inhalation conditions (Zhang et al., 2006a,b) (Zhang et al., 2006a; Zhang et al., 2006b). Figure 10 depicts the evolution of both trajectories and diameters in the oral airways, considering four different isotonic saline droplets (NaCl ≈ 0.9%) at Q_{in}=30 l/min, RH_{in}=60% and T_{in}=303K. Clearly, the diameter of each droplet, starting at the mouth inlet, decreases gradually due to mass loss by evaporation, and then may increase due to water condensation by hygroscopicity, driven by the airflow field and convective heat/mass transfer. Affected by the highly non-uniform, occasionally turbulent airflow structures in the oral airways,

the trajectories for different droplets vary; hence, the changes of droplet diameters are different because of the different local airflow as well as heat and mass transfer. Even when starting with the same diameters, i.e., 3 and 7μm, but different release positions, they undergo contrasting changes depending upon local (moist) environment. Specifically, the diameter of droplet #1 gradually decreases to about 5.5 μm from the mouth inlet to the glottis due to vaporization; however, it may increase slightly in the trachea when it moves near the airway wall where RH_∞ is very high. Droplet #2 may decrease from 7μm to 2.6μm before it starts to grow after the trachea. Small-size droplets (say, d_p=3μm, i.e., droplets #3 and #4) may continuously shrink from the inlet until reaching an equilibrium size where they are neither losing nor absorbing water, and then they start to grow or shrink as they move through a high- or low- humidity environment.

Fig. 10: Trajectories and diameter evolution of selected isotonic saline droplets in the oral airway model with Q_{in}=30 l/min, T_{in}=303K and RH_{in}=60%.

The increase of initial solute concentration for multi-component droplets (e.g., hypertonic saline droplets) may reduce solution (e.g., water) evaporation and increase its condensation (i.e., hygroscopic effects) at droplet surfaces so that the droplet deposition may increase due to the increasing particle diameter and density (Zhang et al., 2006a).

1.3.5 Impact of airway wall absorption on vapor deposition

As mentioned in Sect. 1.2.2, the vapor absorption and uptake in the tissue can be described by Eq. (1); hence, the vapor deposition at the airway surface (mucus layer) is related to a wall absorption parameter K (see Eqs. 2 and 3). The absorption parameter K for different compounds of JP-8 fuel may vary from 10^{-3} to 10^{3}, resulting in large variations of the deposition fractions. Figure 11a shows the variation of deposition fraction in the oral and bifurcation airway models as a function of K. When K is less than one, the deposition is very low in the upper airways due to the low solubility of species in the mucus layer. The deposition fraction is greatly dependent on K for 1<K<1000. If K>1000, the deposition fraction is very close to that for the perfectly absorbing wall condition (i.e., $Y_{wall}=0$). The impact of K on the species mass transfer coefficients in the airways are depicted in Fig. 11b. Clearly, K almost has no effects on the mass transfer coefficients of species with the same diffusivities.
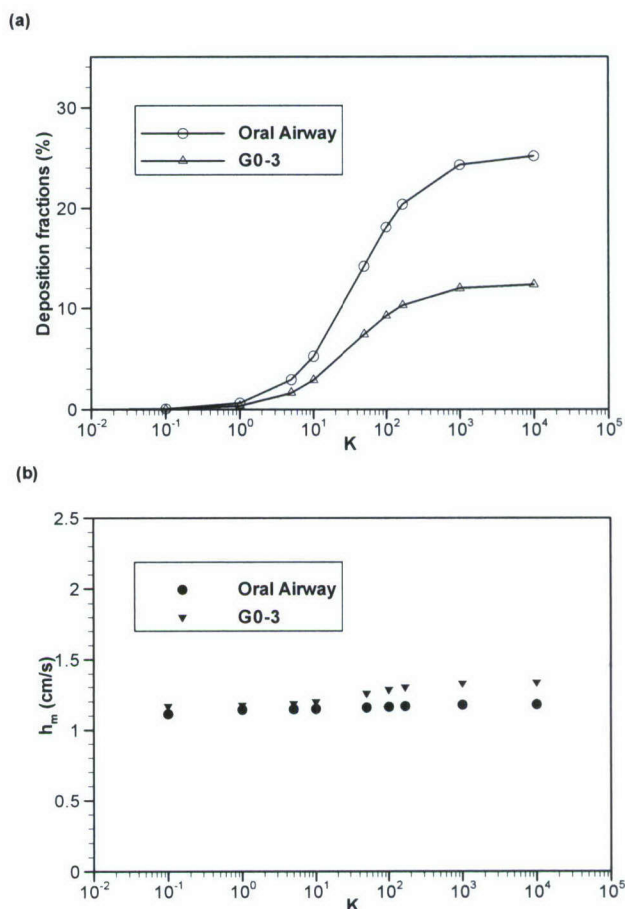
(a)

(b)

Fig. 11: The effects of airway wall absorption parameter K on: (a) JP-8 fuel vapor deposition fraction and (b) mass transfer coefficients in the human upper airway model with Q_{in}=30 l/min.

1.3.6 A new methodology for targeting drug-aerosols in the human respiratory system

Inhalation of medicine for the treatment of lung and other diseases is becoming more and more a preferred option when compared to injection or oral intake. Unfortunately, existing devices such as the popular pressurized metered dose inhalers and dry powder inhalers have rather low deposition efficiencies and their drug-aerosol deliveries are non-directional. This is acceptable when the medicine is inexpensive and does not cause systemic side effects, as it may be the case for patients with mild asthma. However, the delivery of aggressive chemicals, or expensive insulin, vaccines and genetic material embedded in porous particles or droplets requires optimal targeting of such inhaled drug-aerosols to predetermined lung areas. The new methodology introduces the idea of a controlled air-particle stream which provides maximum, patient-specific drug-aerosol deposition based on optimal particle diameter and density, inhalation waveform, and particle-release position. The efficacy of the new methodology is demonstrated with experimentally validated computer simulations of two-phase flow in a human oral airway model with two different sets of tracheobronchial airways (see Fig. 12) (Kleinstreuer et al., 2007). Physical insight to the dynamics of the controlled air-particle stream is provided as well (see Fig. 13) (Kleinstreuer et al., 2008). As shown in Fig. 12, with the controlled inlets
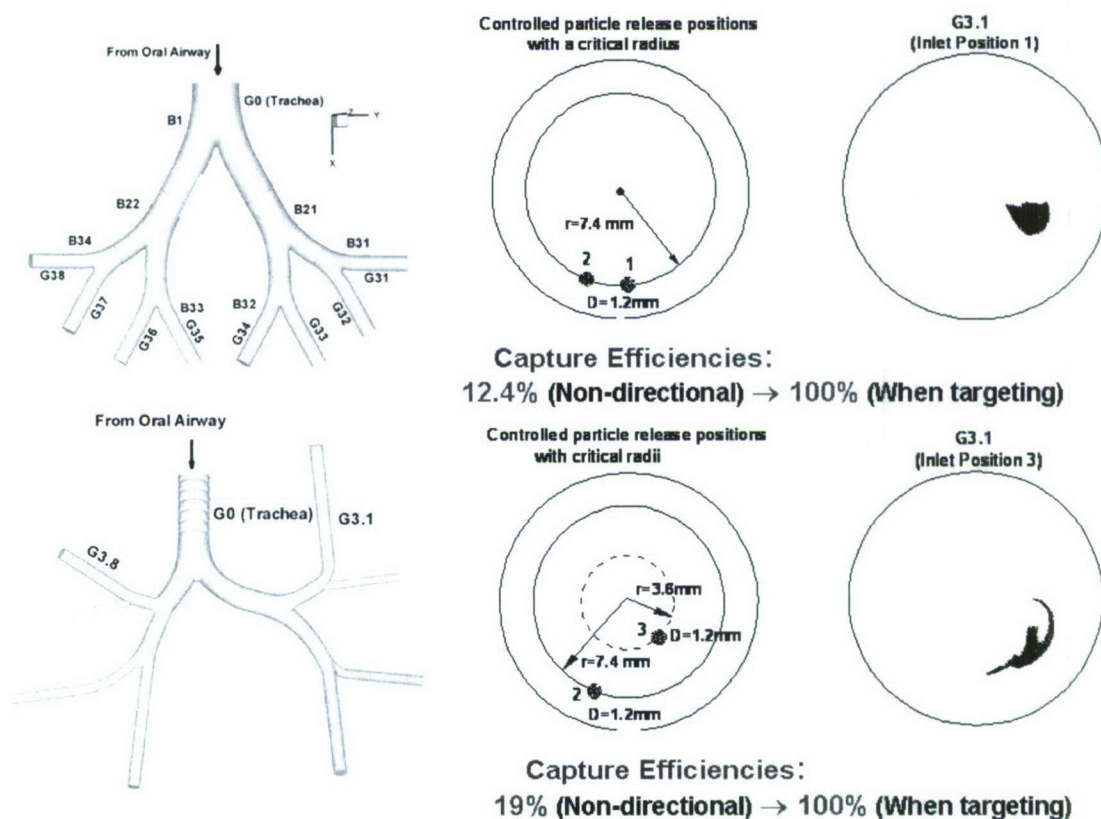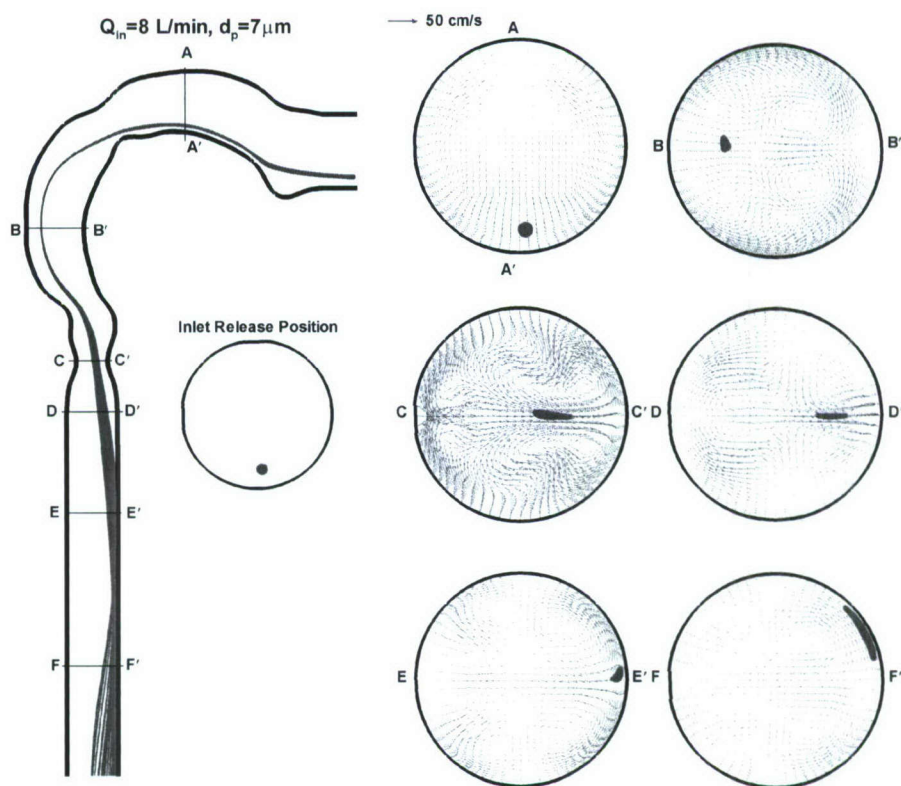

Fig. 12: Demonstration of G-3 outlets of idealized and realistic airways targeting.

(Inlet positions #1 and 3), the capture efficiency of particles in the targeted areas (e.g., G3.1 exit) can increase from about 10%~ 20% to 100%, no matter an idealized or a realistic airway model is employed. Distributions of particles entering targeted (outlet) airways are mainly driven by secondary flows. Figure 13 depicts an example of transport of a micron particle stream in the oral airway model driven by laminar airflow.

In summary, drug-aerosols have typically effective diameters of $1\mu m$ to $20\mu m$, a size range which precludes Brownian motion and high impaction parameter values; hence, they tend to follow local streamlines. The determination of suitable particle release positions for optimal site-specific targeting is the most important element of the new methodology, which is achieved via "backtracking".

Fig. 13: Distributions of particles released from a given mouth inlet position with $Q_{in}=8$ L/min and $d_p=7\mu m$ at the oral airway model. The left panel exhibits the particle trajectories while the right panel depicts particle distributions and secondary velocity vectors at different cross sections.

1.4 CONCLUSIONS AND SUMMARY OF ACCOMPLISHMENTS

Using representative human nasal, oral and tracheobronchial airway models, transient 3-

D as well as *equivalent* steady-state solutions have been obtained for the transport and deposition of spherical particles and droplets as well as vapors. It should be noted that equivalence to transient airflow and particle deposition results was achieved by employing matching Reynolds and Stokes numbers for steady-state simulations. *Inhalation inlet conditions and aerosol characteristics resembled JP-8 fuel exposure scenarios in most case studies.* Key multi-scale computational analysis and simulation results can be summarized as follows.

(i) Airflow and Transport and Deposition of Micron- and Nano-size Aerosols in Representative Human Nasal Airways:

(a) The unique flow characteristics, such as flow separation, and secondary flows, in representative human nasal cavities have been simulated systematically. Detailed local deposition patterns and deposition efficiencies of nanoparticles and equivalent JP-8 fuel vapors have been studied.

(b) Wall roughness of nasal cavities was found to have a significant effect on deposition of micron particles with a diameter larger than 4 μm. With the correction for wall roughness, the micron particle deposition efficiency in the nasal airway was successfully simulated for the first time when compared to measured data sets (see Fig.1).

(ii) Multi-component and/or Impure Droplet Evaporation or Hygroscopicity: A semi-empirical evaporation model in conjunction with the identified surrogate mixture provide a computationally efficient method for computing JP-8 fuel droplet evaporation that can track individual toxic markers. Impurities of droplets may reduce the surface vapor pressure and hence decrease droplet evaporation or cause droplet growth. In both scenarios, droplet trajectories and deposition locations/efficiencies are influenced by varying droplet diameters.

(iii) Deposition Differences between Fuel Aerosols (i.e., Droplets) vs. Vapors: Deposited vapor coats much more uniformly the airway surfaces when compared to droplet deposition. The maximum ratio of cellular deposition to average surface deposition for vapors may be two orders smaller than for droplets. This may imply different toxicities and even higher toxicities for vapors due to potentially augmented translocation of vapor molecules into tissues because of more uniform, large-area deposition distributions. In addition, airway wall absorption may greatly influence the fuel vapor deposition in different parts of the lungs. For example, the low resistance and thin liquid lining-layer in lower airways (or the alveolar region) may cause more vapor deposition than that in the upper airways.

(iv) Lattice-Boltzmann Method (LBM) Analyses of Airflow and Micron Particle Transport/Deposition in Transient 2-D Alveolar Models with Moving Boundaries: A computer program based on LBM has been successfully developed in house. Airflow

and microparticle transport in 2-D alveolar ducts with expanding/contracting sacs have been simulated and verified.

(v) Steady/Transient Airflow and Micron Particle Transport in Representative Asymmetric Tracheobronchial Airways: The effects of airway asymmetry and the presence of tracheal rings on airflow and particle deposition have been simulated and discussed, using an in-house finite-volume solver, which now also runs on ARL's HPC.

(vi) Studies of JP-8 Fuel Vapor Transport and Deposition by Considering Airway Wall Absorption: The respiratory uptake of vapors of different fuel components is greatly influenced by airway wall absorption in terms of a dimensionless absorption parameter K. The deposition is very low in the upper airways when K is less than one and the deposition fraction is very close to that assuming a perfectly absorbing wall when K>1000. Thus, the deposition fraction is greatly dependent on materials, i.e., fuel components, with 1<K<1000. The deposition is greater for vapors with higher diffusivity and solubility. The parameter K has almost no effect on the mass transfer coefficients of species with the same diffusivities. Thus, the mass transfer coefficients of vapors in the upper airway can be correlated as a function of flow and diffusion parameters.

(vii) Optimal Drug-Aerosol Targeting: Commonly used inhalers are non-directional and at best only regional drug-aerosol deposition can be achieved. However, when inhaling expensive and aggressive medicine, or critical lung areas have to be reached, locally targeted drug-aerosol delivery is imperative. For that reason the underlying principle of a future line of "smart inhalers" is introduced. Specifically, by generating a controlled air-particle stream, most of the inhaled drug aerosols reach predetermined lung sites, which are associated with specific diseases and/or treatments. Using the same human upper airway model, experimentally confirmed computer predictions of controlled particle transport from mouth to generation 3 are provided.

Clearly, once appropriate drugs have been developed to treat (or even prevent) detrimental effects of JP-8 fuel inhalation, the use of smart inhaler systems, based on the new targeting methodology, should be beneficial.

References

Agency for Toxic Substances and Disease Registry (ATSDR), 2005. Toxicological Profile for Naphthalene, 1-Methylnaphthalene, and 2-Methylnaphthalene. US Department of Health and Human Services.

Balashazy, I., Hofmann, W., Heistracher, T., 2003. Local particle deposition patterns may play a key role in the development of lung cancer. Journal of Applied Physiology 94, 1719-1725.

Broday, D.M., 2004. Deposition of ultrafine particles at carinal ridges of the upper bronchial airways. Aerosol Science and Technology 38, 991-1000.

Comer, J.K., Kleinstreuer, C., Hyun, S., Kim, C.S., 2000. Aerosol transport and deposition in sequentially bifurcating airways. Journal of Biomechanical Engineering – Trans of the ASME 122, 152-158.

Comer, J.K., Kleinstreuer, C., Zhang, Z., 2001. Flow structures and particle deposition patterns in double-bifurcation airway models. Part 1. Air flow fields. Journal of Fluid Mechanics 435, 25-54.

Edwards, T. & Maurice, L. Q., 2001. Surrogate mixtures to represent complex aviation and rocket fuels, Journal of Propulsion and Power 17(2), 461-466.

Fan, B.J., Cheng, Y.S., Yeh, H.C., 1996. Gas collection efficiency and entrance flow effect of an annular diffusion denuder. Aerosol Science and Technology 25, 113-120.

Frampton, MW, 2001. Systemic and cardiovascular effects of airway injury and inflammation: Ultrafine particle exposure in humans. Environmental Health Perspectives, 109 (Suppl. 4), 529-532.

Fresconi, F.E., Wexler, A.S., & Prasad, A.K., 2003. Expiration flow in a symmetric bifurcation. Experiments in Fluids, 35, 493-501.

Gehr, P. & Heyder, J. (Ed.) (2000). *Particle-Lung Interaction*, New York: Marcel Dekker.

Haefelibleuer, B., Weibel, E.R., 1988. Morphometry of the Human Pulmonary Acinus. Anatomical Record 220, 401-414.

Hoet, P., Brueske-Hohlfeld, I., Salata, O., 2004. Nanoparticles – known and unknown health risks. Journal of Nanobiotechnology 2, 12.

Kelly, J.T., Asgharian, B., Kimbell, J.S., Wong, B.A., 2004. Particle deposition in human nasal airway replicas manufactured by different methods. Part I: Inertial regime particles. Aerosol Science and Technology 38, 1063-1071.

Keyhani, K., Scherer, P.W., Mozell, M.M., 1997. A numerical model of nasal odorant transport for the analysis of human olfaction. Journal of Theoretical Biology 186, 279-301.

Kleinstreuer, C., Shi, H., Zhang, Z., 2007. Computational analyses of a pressurized metered dose inhaler and a new drug-aerosol targeting methodology. Journal of Aerosol Medicine-Deposition Clearance and Effects in the Lung 20, 294-309.

Kleinstreuer, C., Zhang, Z., 2003. Laminar-to-turbulent fluid-particle flows in a human airway model. International Journal of Multiphase Flow 29, 271-289.

Kleinstreuer, C., Zhang, Z., Li, Z., Roberts, W.L., and Rojas, C., 2008, A New Methodology for Targeting Drug-Aerosols in the Human Respiratory System. International Journal of Heat and Mass Transfer, in press.

Li, Z., Kleinstreuer, C., 2007. Alveolar Flow Analyses using the lattice Boltzmann Method. Journal of Computational Physics, in review.

Li, Z., Kleinstreuer, C., Zhang, Z., 2007. Particle deposition in the human tracheobronchial airways due to transient inspiratory flow patterns. Journal of Aerosol Science 38, 625-644.

Longest, P.W., Kleinstreuer, C., 2005. Computational models for simulating multicomponent aerosol evaporation in the upper respiratory airways. Aerosol Science and Technology 39, 124-138.

Mala, G.M., and Li, D., 1999. Flow characteristics of water in microtubes, International Journal of Heat and Fluid Flow 20, 142-148

National Research Council (NRC). Board on Environmental Studies of Toxicology (BEST). 2003. *Toxicologic assessment of jet-propulsion fuel-8.* Washington, DC: National Academy Press.

Oberdorster, G., Oberdorster, E., Oberdorster, J., 2005. Nanotoxicology: An emerging discipline evolving from studies of ultrafine particles. Environmental Health Perspectives 113, 823-839.

Ritchie, G., Still, K., Rossi III, J., Bekkedal, M., Bobb, A. and Arfsten, D., 2003. Biological and health effects of exposure to kerosene-based jet fuels and performance additives. J. Toxicol. Environ. Health B: Crit. Rev. 6, 357–451.

Runge, T., Meske, M., and Polymeropoulou, C. E., 1998. Low-Temperature Vaporization of JP-4 and JP-8 Fuel Droplets, Atomization Sprays 8, 25–44.

Shi, H., Kleinstreuer, C., Zhang, Z., 2006. Laminar airflow and nanoparticle or vapor deposition in a human nasal cavity model. Journal of Biomechanical Engineering-Transactions of the ASME 128, 697-706.

Shi, H., Kleinstreuer, C., Zhang, Z., 2007a. Modeling of inertial particle transport and deposition in human nasal cavities with wall roughness Journal of Aerosol Science 38, 398-419.

Shi, H., Kleinstreuer, C., Zhang, Z., Kim, C.S., 2004. Nanoparticle transport and deposition in bifurcating tubes with different inlet conditions. Physics of Fluids 16, 2199-2213.

Shi, H.., Kleinstreuer, C., Zhang, Z., 2007b. Modeling of inertial particle transport and deposition in human nasal cavities with wall roughness. Journal of Aerosol Science 38, 398-419.

Shi, H., Kleinstreuer, C., and Zhang, Z., 2008, Nanofluid Flow and Nanoparticle Deposition in a Human Nasal Airway Model, Physics of Fluids, in press.

Singh, N. & Davis, G.S., 2002. Review: occupational and environmental lung disease. Current Opinion in Pulmonary Medicine, 8(2), 117-125.

Weibel, E.R., 1963. *Morphometry of the Human Lung*. Academic Press, New York.

Wilcox, D.C., 1998. *Turbulence Modeling for CFD* DCW Industries, Inc, LA Canada, CA.

Zhang, Z., Kleinstreuer, C., 2002. Transient airflow structures and particle transport in a sequentially branching lung airway model. Physics of Fluids 14, 862-880.

Zhang, Z., Kleinstreuer, C., 2003a. Low-Reynolds-number turbulent flows in locally constricted conduits: A comparison study. AIAA Journal 41, 831-840.

Zhang, Z., Kleinstreuer, C., 2003b. Species heat and mass transfer in a human upper airway model. International Journal of Heat and Mass Transfer 46, 4755-4768.

Zhang, Z., Kleinstreuer, C., 2004. Airflow structures and nano-particle deposition in a human upper airway model. Journal of Computational Physics 198, 178-210.

Zhang, Z., Kleinstreuer, C., Donohue, J.F., Kim, C.S., 2005. Comparison of micro- and nano-size particle depositions in a human upper airway model. Journal of Aerosol Science 36, 211-233.

Zhang, Z., Kleinstreuer, C., Kim, C.S., 2001a. Effects of curved inlet tubes on air flow and particle deposition in bifurcating lung models. Journal of Biomechanics 34, 659-669.

Zhang, Z., Kleinstreuer, C., Kim, C.S., 2001b. Flow structure and particle transport in a triple bifurcation airway model. Journal of Fluids Engineering-Transactions of the ASME 123, 320-330.

Zhang, Z., Kleinstreuer, C., Kim, C.S., 2002a. Aerosol deposition efficiencies and upstream release positions for different inhalation modes in an upper bronchial airway model. Aerosol Science and Technology 36, 828-844.

Zhang, Z., Kleinstreuer, C., Kim, C.S., 2002b. Cyclic micron-size particle inhalation and deposition in a triple bifurcation lung airway model. Journal of Aerosol Science 33, 257-281.

Zhang, Z., Kleinstreuer, C., Kim, C.S., 2002c. Gas-solid two-phase flow in a triple bifurcation lung airway model. International Journal of Multiphase Flow 28, 1021-1046.

Zhang, Z., Kleinstreuer, C., Kim, C.S., 2002d. Micro-particle transport and deposition in a human oral airway model. Journal of Aerosol Science 33, 1635-1652.

Zhang, Z., Kleinstreuer, C., Kim, C.S., 2006a. Isotonic and hypertonic saline droplet deposition in a human upper airway model. Journal of Aerosol Medicine-Deposition Clearance and Effects in the Lung 19, 184-198.

Zhang, Z., Kleinstreuer, C., Kim, C.S., 2006b. Water vapor transport and its effects on the deposition of hygroscopic droplets in a human upper airway model. Aerosol Science and Technology 40, 1-16.

Zhang, Z., Kleinstreuer, C., Kim, C.S., Cheng, Y.S., 2004. Vaporizing microdroplet inhalation, transport, and deposition in a human upper airway model. Aerosol Science and Technology 38, 36-49.

2. Publications

Journal Articles:

1. Zhang, Z., Kleinstreuer, C., Kim, C. S. and Cheng, Y. S., 2004, "Vaporizing Micro-Droplet Inhalation, Transport and Deposition in a Human Upper Airway Model", *Aerosol Science and Technology*, Vol.38, 36-49.

2. Zhang, Z., and Kleinstreuer, C, 2004, "Airflow Structures and Nano-Particle Deposition in a Human Upper Airway Model", *Journal of Computational Physics*, Vol. 198, 178-210.

3. Longest, P.W. and Kleinstreuer, C., 2004, "Interacting Effects of Uniform Flow, Plane Shear, and Near-Wall Proximity on the Heat and Mass Transfer of Respiratory Aerosols", International Journal of Heat and Mass Transfer, Vol. 47, 4745-4759.

4. Zhang, Z., Kleinstreuer, C, Donohue, J.F. and Kim, C. S., 2005, "Comparison of Micro- and Nano-Size Particle Depositions in a Human Upper Airway Model", Journal of Aerosol Science, Vol. 36(2), 211-233.

5. Longest, P.W. and Kleinstreuer, C., 2005, "Computational Models for Simulating Multicomponent Aerosol Evaporation in the Upper Respiratory Airways", Aerosol Science and Technology, 39: 124-138.

6. Zhang, Z., Kleinstreuer, C., and Kim, C.S., 2006, "Water Vapor Transport and Its Effects on the Deposition of Hygroscopic Droplets in a Human Upper Airway Model", Aerosol Science & Technology, 40: 52-67.

7. Zhang, Z., Kleinstreuer, C., and Kim, C.S., 2006, "Isotonic and Hypertonic Saline Droplet Deposition in a Human Upper Airway Model", Journal of Aerosol Medicine, 19 (2): 184-198.

8. Shi, H., Kleinstreuer, C., and Zhang, Z., 2006, "Laminar Airflow and Ultrafine-Particle Deposition in a Human Nasal Cavity Model", ASME Journal of Biomechanical Engineering, Vol. 128, 697-706.

9. Kleinstreuer, C., Zhang, Z. and Kim, C.S., 2007, "Combined inertial and gravitational deposition of microparticles in small model airways of the human respiratory system," *Journal of Aerosol Science*, 38(10): 1047-1061.

10. Li, Z., Kleinstreuer, C., and Zhang, Z., 2007, "Particle deposition in the human tracheobronchial airways due to transient inspiratory flow patterns," *Journal of Aerosol Science*, 38(6): 625-644.

11. Li, Z., Kleinstreuer, C. and Zhang, Z., 2007, "Simulation of Airflow Fields and Microparticle Deposition in Realistic Human Lung Airway Models, Part I: Airflow Patterns, *European Journal of Mechanics B/Fluid*, 26: 632-649.

12. Li, Z., Kleinstreuer, C. and Zhang, Z., 2007, "Simulation of Airflow Fields and Microparticle Deposition in Realistic Human Lung Airway Models Part II: Particle Transportation and Deposition", *European Journal of Mechanics B/Fluid*, 26: 650-668.

13. Kleinstreuer, C., Shi, H., and Zhang, Z., 2007, "Computational Analyses of a Pressurized Metered Dose Inhaler and a New Drug-Aerosol Targeting Methodology", *Journal of Aerosol Medicine*, 20(3): 294-309.

14. Shi, H., Kleinstreuer, C., and Zhang, Z., 2007, "Modeling of inertial particle transport and deposition in human nasal cavities with wall roughness," *Journal of Aerosol Science*, 38: 398-419.

Articles In Press and Submitted:

15. Shi, H., Kleinstreuer, C., and Zhang, Z., 2008, "Nanofluid Flow and Nanoparticle Deposition in a Human Nasal Airway Model," *Physics of Fluids*, in press.

16. Kleinstreuer, C., Zhang, Z., and Donohue, J.F., 2008, "Targeted Drug-aerosol Delivery in the Human Respiratory System," *Annual Review of Biomedical Engineering*, Vol. 10 (on-line April 2008).

17. Kleinstreuer, C., Zhang, Z., and Li, Z., 2008, "Modeling Airflow and Particle Transport/Deposition in Pulmonary Airways", Invited Review Paper for *Respiratory Physiology & Neurobiology*.

Conference Papers and Workshop Presentations:

1. Zhang, Z., Kleinstreuer, C. and Kim, C.S., 2004, "Computational Analysis of Micro- and Nano- Particle Deposition in Human Tracheobronchial Airways", *23rd Annual Conference of the American Association for Aerosol Research* (AAAR), Atlanta, Georgia, Oct. 5-8.

2. Shi, H., Kleinstreuer, C., Zhang, Z. and Kim, C. S. 2004, "Numerical Simulation of Inspiratory Airflow and Nanoparticle Transport and Deposition in the Human Nasal Cavity", *23rd Annual Conference of the American Association for Aerosol Research* (AAAR), Atlanta, Georgia, Oct.5-8.

3. Kleinstreuer, C., Zhang, Z., and Shi, H., 2005, "Computational Analyses of JP-8 Fuel Droplet and Vapor Depositions in Human Upper Airway Models," 2005 JP-8 Jet Fuel Exposure and Health Effects Symposium, Tucson, AZ, 30 November -2 December.

4. Kleinstreuer, C., 2006, "Modeling the Deposition of Jet Fuel Aerosol Particles in the Respiratory Track of Humans," Jet Fuel Meeting: Integrating Models on Lung Deposition and Toxicokinetics of Jet Fuels," North Carolina State University, Raleigh, NC, Jan. 24, 2006.

5. Kleinstreuer, C., Shi, H., and Zhang, Z., 2006, "Computational Analysis of Nanoparticle

Transport and Deposition in Models of the Human Respiratory System," Work-in-Progress Meeting for the AFOSR Nanotoxicology Program at the University of Rochester, Rochester, NY, May 16, 2006.

6. Li, Z., and Kleinstreuer, C., 2006, "Fluid-Structure Interactions and Particle Transport/Deposition in an Alveolated Bifurcation using the Lattice Boltzmann Method," 3rd ICMMES Conference at the Radisson Hotel Hampton, Norfolk, VA, USA, July 24-28.

7. Li, Z., Kleinstreuer, C., and Zhang, Z., 2007, "Computational Analyses of JP-8 Fuel Aerosol Deposition in Human Upper Airway," JP-8 Jet Fuel Exposure and Health Effects Symposium, Tucson, AZ, 17 January -21 January.

8. Zhang, Z., and Kleinstreuer, C., 2007, "Micro- And Nano- Particle Deposition In Human Tracheobronchial Airways", *26th Annual Conference of the American Association for Aerosol Research* (AAAR), Reno, NV, Sept. 24-28.

9. Li, Z., Kleinstreuer, C., and Zhang, Z., 2007, "Airflow and Micron Particle Transport/Deposition in Different Human Lung Airway Models," *26th Annual Conference of the American Association for Aerosol Research* (AAAR), Reno, NV, Sept. 24-28.

(PDF files of Journal Articles are attached).

3 Follow-On Uses: Technology Assists, Transitions, or Transfers

(a) New, easy-to-use correlations for nanoparticle depositions in both the human nasal cavities and upper airways have been developed and checked against measured data sets.

(b) Three research reports with our findings on the transport and deposition of toxic solid particles as well as evaporating droplets in lung airway models have been delivered to Dr CS Kim (US EPA, kim.chong@epa.gov) for use by toxicologists, regulators, etc. Specifically, we simulated and validated "nanoparticle deposition in a representative nasal airway model", "micron particle transport and deposition in human nasal airways", and "combined inertial and gravitational deposition of microparticles in small human airways".

(c) The virtual reality work on the smart inhaler system (SIS), which was a secondary outcome of the AFOSR-sponsored research since 2001, attracted some small NIH support for proof-of-concept work, including start-up to build a prototype, involving the PI's colleagues Drs Roberts and Seelecke. A US and international patent applications for the SIS has been submitted (see Kleinstreuer, C and Seelecke, S., 2006, "Inhaler System for Targeted Maximum Drug-Aerosol Delivery", US and PCT patent applications (297/215/2) by Jim Daly for NC State University (05-096)). In collaboration with the PI, laboratory proof-of-concept was obtained by Dr Roberts and his graduate student.

(Attached Excel file: Follow-on Uses.xls)

4. Accomplishments and Successes

The main accomplishments/key findings are summarized in Sect.1.4. These results are also documented in 17 peer-reviewed journal articles (14 published and 3 accepted or submitted) and 9 conference papers/presentations. In addition:

(a) Our paper "Comparison of Micro- and Nano-Size Particle Depositions in a Human Upper Airway Model" Journal of Aerosol Science, 36 (2005) 211-233, has been listed as one of most requested articles (Top 25) (April 2004 - March 2005) in the Journal of Aerosol Science (http://www1.elsevier.com/homepage/sad/downloads/00218502.html).

(b) Our journal articles, based on the AFOSR-sponsored research efforts since 2001, have been cited by other researchers more than 300 times (Source: Web of Science).

(Attached Excel file: Accomplishments.xls)

5. Professional Personnel Supported

- **PI Dr. Clement Kleinstreuer,** Professor　　　　　(20%, 3years)
- **Dr. Zhe Zhang,** Research Associate Professor　　　($80 \sim 100\%$, 3 years)
- **Wei Shi,** Graduate student (RA)　　　　　　　　(50%, 2 years)
- **Zheng Li,** Graduate student (RA)　　　　　　　(50%, 3 years)

6. Honors and Awards Received

None

7. Professional Activities

Dr. Clement Kleinstreuer:

- Associate Editor of Int'l J. Energy Systems

- NSF Review Panel (BES Division), NIH Review Panel (NHLBI)

- Scientific Committee Member of ICMF-2004 (Japan)

- Consultant to: Glaxo-Smith-Kline (Pharmac. Clean Room), RTP, NC; W.L. Gore & Assoc. (Medical Division) Flagstaff, AZ; IMPRA, Inc. (Graft Optimization) Tempe, AZ; U.S. EPA (Lung Aerosol Deposition), RTP, NC; Bespak (Drug Aerosol Delivery), Apex, NC

- Fellow of NC Supercomputing Center Research Institute; Member of American Society of Mechanical Engineers, Biomedical Engineering Society, American Association of Aerosol Research

- Reviewer of numerous fluid mechanics, aerosol science, two-phase flow, and biomedical engineering journal papers.

Dr. Zhe Zhang:

- Reviewer for Physics of Fluids, Annals of Biomedical Engineering, Aerosol Science & Technology, Inhalation Toxicology, ASME J. Biomechanical Engineering, Journal of Aerosol Science, Respiratory Physiology & Neurobiology, ASME J. Heat Transfer, Continuum Mechanics and Thermodynamics
- Member of American Association of Aerosol Research